Gelation Kinetics of β-Hairpin Peptide Hydrogel Networks

Cecile Veerman,[†] Karthikan Rajagopal,[‡] Chandra Sekhar Palla,[†] Darrin J. Pochan,[§] Joel P. Schneider,[‡] and Eric M. Furst*,[†]

Department of Chemical Engineering, Department of Chemistry and Biochemistry, and Department of Materials Science and Engineering, University of Delaware, Newark, Delaware 19716

Received April 27, 2006; Revised Manuscript Received July 21, 2006

ABSTRACT: The gelation kinetics of self-assembled hydrogels consisting of the β-hairpin peptide MAX1 are investigated using microrheology and far-UV circular dichroism (CD) spectroscopy. The intramolecular folding of this peptide is engineered to control its self-assembly into β-sheet-rich hydrogels. When the peptide is unfolded, it does not self-assemble, and aqueous solutions have the viscosity of water. Folding and consequent self-assembly are triggered by changes in pH, temperature, or ionic strength. This folding and self-assembly mechanism allows temporal control of the material formation. CD spectroscopy shows that the kinetics of β-sheet structure formation occurs in a concentration-dependent manner but does not provide information on the kinetics of network assembly. Here, multiple particle tracking is used to define exact gelation times as a function of peptide concentration. This allows an empirical relationship to be established between the rheologically defined gelation time and the onset of β-sheet formation as measured by CD. Values of the mean-residue ellipticity at 216 nm between -10×10^3 and -12×10^3 deg dmol^{-1} cm^2 coincide with the formation of a percolating gel. Critically, this empirical relationship allows one to identify the gel time solely from spectroscopic measurements, greatly facilitating the establishment of peptide sequence material−function relationships.

I. Introduction

Hydrogel networks formed via the self-assembly of oligopeptides and protein polymers offer exciting new possibilities for the rational design of novel materials.[1−10] Such systems have the potential to find wide application in microfluidics,[11,12] drug delivery,[13−15] and tissue engineering.[16−18] Properties specific to tissue engineering, such as biocompatibility, biodegradability, and remodeling characteristics, are dependent on the environmental responsiveness of the material. Thus, recent research has focused on using small peptide sequences that self-assemble into materials, and peptides can be engineered such that the formation and final properties display responsive behavior. For example, Schneider and Pochan have successfully engineered a family of β-hairpin peptides that undergo self-assembly in response to changes in pH,[1] temperature,[19] ionic strength,[20] cell culture media,[21] or photoinitiation.[22] For these peptides, the ability to self-assemble is linked to the unimolecular folded conformation. When the peptide is unfolded, it does not self-assemble, and aqueous solutions have the viscosity of water. Triggered intramolecular folding results in the formation of amphiphilic β-hairpins that are prone to an intermolecular, hierarchical, self-assembly process.

MAX1 is a 20-residue peptide composed of an alternating sequence of high β-sheet propensity valine and lysine residues[1] flanking a central tetrapeptide designed to adopt a type II′ turn structure (Figure 1). Electrostatic interactions between residue side chains can be manipulated to initiate folding and assembly, leading to hydrogel formation. For example, under acidic conditions, the lysine side chains of MAX1 are protonated, which prevents peptide folding and self-assembly. Intramolecular folding can be triggered either by screening some of the lysine-based charge with salt at physiological pH or by neutralizing the lysine point charges by increasing the pH of low ionic strength solutions to 9. Consequent self-assembly results in a three-dimensional hydrogel network formed via hydrophobic association of the valine-rich faces of two β-hairpins and extensive intermolecular hydrogen bonding networks.[1,19,23] These networks consist of filamentous structures on the nanoscale, as determined using electron microscopy and small- and ultrasmall-angle neutron scattering.[23]

Spectroscopic measurements, such as circular dichroism (CD), have typically been used to monitor the folding of such peptides. Filament formation and subsequent gelation are fully dependent on the folded state of the peptide. This implies a direct relationship between the extent of β-sheet formation measured by CD spectroscopy to the evolution of network structure. However, it is nearly impossible to deconvolute a typical β-sheet spectrum into separate contributions from the monomer and assembled macromolecular structures of different sizes. Therefore, from CD spectroscopy alone, one cannot distinguish the degree that the folded peptide has been incorporated into the growing assembly and the exact time that a sample-spanning, percolated hydrogel network is formed. Defining this percolation time, or gel point, is essential for exploring structure−material formation relationships to identify optimal sequences for applications, including cell encapsulation.

Rheological measurements are an excellent candidate to measure the transient and steady-state structural and mechanical properties of soft complex materials, including peptide hydrogels.[1] The transition from a liquidlike to a solidlike behavior depends solely on the formation of the growing self-assembled peptide microstructure and is largely insensitive to the transition of the peptide from the unfolded to the folded state. This provides access to the kinetics of the network assembly that cannot be determined by CD. However, measurements of the gelation kinetics using *bulk* rheology are complicated for the systems studied here by the rapid self-assembly kinetics. For instance, previous macroscopic rheological experiments for 2

[†] Department of Chemical Engineering.
[‡] Department of Chemistry and Biochemistry.
[§] Department of Materials Science and Engineering.
* Corresponding author: e-mail furst@che.udel.edu; Tel +1 (302) 831-0102; Fax +1 (302) 831-1048.

10.1021/ma0609331 CCC: $33.50
Published on Web 08/26/2006

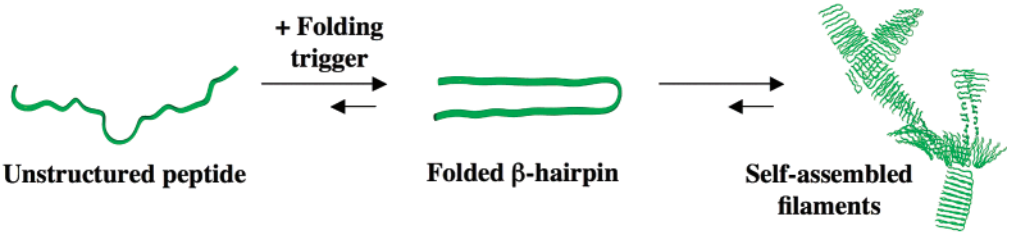

Figure 1. MAX1 folding and self-assembly.

wt % MAX1 demonstrate that the elastic properties develop quickly with time.[1] At these higher concentrations, the kinetics are rapid enough that the initial assembly and gelation kinetics cannot be resolved. At the earliest accessible experimental times after initiating peptide folding, the self-assembled network is already past the percolation point.

In contrast to bulk rheology, microrheology[24−27] enables us to characterize the gelation kinetics of more slowly assembling gels formed at low peptide concentrations. Because of the weakness of the gels at low concentrations, bulk rheological measurements are limited in this regime by poor signal-to-noise, especially for resolving the elastic properties of the growing microstructure before the gel point is reached.

Passive microrheological techniques, such as multiple particle tracking,[25,28] measure the thermal motion of tracer particles embedded in a complex fluid. When the thermally driven tracer particles are large compared to the microstructural length scales of the surrounding medium, the ensemble-averaged mean-squared displacement ($\langle \Delta r^2(t) \rangle$), calculated from the probe particle trajectories, is directly related to the linear viscoelastic properties by the generalized Stokes−Einstein relation (GSER), written here in terms of the creep compliance $J(t)$[29]

$$\langle \Delta r^2(t) \rangle = \frac{k_B T}{\pi a} J(t) \tag{1}$$

where k_BT is the thermal energy and a is the probe particle radii.[24,26,30] $J(t)$ relates the material strain deformation $\gamma(t)$ to the rate of applied stress $\dot{\sigma}(t)$ via $\gamma(t) = \int_0^t J(t - t')\dot{\sigma}(t)\, dt'$.[31] Equation 1 provides a straightforward physical interpretation of microrheology; the mean-squared displacement represents a strain deformation caused by an average thermal stress from Brownian fluctuations of the surrounding material.[32] Therefore, by measuring the change in the mean-squared displacement as a function of time after peptide assembly is initiated, one can monitor the evolving viscoelastic properties of the developing hydrogel network.[33]

II. Experimental Section

A. Sample Preparation. Methods for peptide synthesis and purification are given elsewhere.[1] For the multiple particle tracking experiments, a 1% MAX1 stock solution was obtained by dissolving lyophilized MAX1 in Milli-Q water. From this stock solution, required amounts of MAX1 were taken with final concentrations MAX1 of 0.05−0.15%. Fluorescent polystyrene (PS) microspheres (Polysciences, Warrington, PA), 1.0 μm in diameter, were added, where the final volume fraction of tracer particles was 0.4%. Control experiments to measure the effect of particle size and surface chemistry were performed using 0.75 and 0.5 μm diameter PS probes and 0.75 and 1.0 μm diameter carboxylated PS particles (PS-COOH, Polysciences). The self-assembly process was initiated by the addition of a buffer stock solution with a final concentration of 125 mM borate and 10 mM NaCl at pH 9.

B. Multiple Particle Tracking. Samples were prepared using standard glass microscope slides (Fisher Scientific, 25 × 75 × 1 mm) on top of which a coverslip (Corning, No 1.5, 22 mm^2) was added, separated by an adhesive spacer. Approximately 45 μL of a solution consisting of MAX1, tracer particles, and buffer was placed at the edge of the coverslip and the slide and was pulled into the cell by capillary forces. When the cell was completely filled with solution, the edges of the coverslip and slide were sealed with a fast UV curing epoxy glue (Norland Products, NOA 81) to prevent drying and convective flow in the sample. Data sets that exhibited drift due to convection were not used in the analysis.

Fluorescent probe particles were imaged with an inverted optical epifluorescence microscope, using a total magnification of 64× (40× objective, and 1.6× tube lens, Axiovert 200, Zeiss, N.A. 0.75). The movement of the particles was recorded with a CCD camera coupled to the microscope (154 nm/pixel) at various times after the self-assembly process was initiated by the addition of buffer. About 100 particles were visible in each image. For each time, ∼10 s of images were acquired at a frame rate of 60 Hz. The positions of the tracer particles were identified in each frame to within 55 nm by finding the brightness averaged centroid position.[34] The positions of the particles were linked in time to obtain two-dimensional particle trajectories. The trajectories are then used to calculate the ensemble-averaged mean-squared displacement $\langle \Delta r^2(t) \rangle$. A sliding 1 s time window is used to increase the number of trajectories used in each average to ∼1000, which is sufficient to acquire consistent and accurate statistics.

C. Laser Tweezer Microrheology. Laser tweezer microrheology was performed by measuring the response of dispersed colloidal polystyrene microspheres that are held by an oscillating optical trap. Details of the experimental apparatus are given elsewhere.[35] Briefly, the particle response to an oscillating optical trap $x_t(t) = A\cos(\omega t)$ with trap stiffness κ_t is $x(t) = D(\omega)\cos[\omega t - \delta(\omega)]$,[36] where

$$D(\omega) = \frac{\kappa_t A}{[(\kappa_t + \kappa_e^*)^2 + (6\pi a \eta^* \omega)^2]^{1/2}} \tag{2}$$

and

$$\tan \delta(\omega) = \frac{6\pi a \eta^* \omega}{\kappa_e^* + \kappa_t} \tag{3}$$

The storage and loss moduli are calculated from the frequency-dependent dynamic elastic $\kappa_e^*(\omega)$ and viscous $\eta^*(\omega)$ contants

$$G'(\omega) = \frac{\kappa_e^*}{6\pi a} = \frac{\kappa_t}{6\pi a}\left[\frac{A\cos\delta(\omega)}{D(\omega)} - 1\right] \tag{4}$$

$$G''(\omega) = \eta^*(\omega)\omega = \frac{\kappa_t A \sin\delta(\omega)}{6\pi a D(\omega)} \tag{5}$$

Values of κ_t typically range between 10 and 50 pN/μm.

D. Circular Dichroism Spectroscopy. Circular dichroism (CD) spectra were collected on a Jasco J-810 spectropolarimeter. A 1 mM stock solution of MAX 1 was prepared, and the concentration was determined by absorbance at 220 nm (ϵ = 15 750 cm^{-1} M^{-1}).

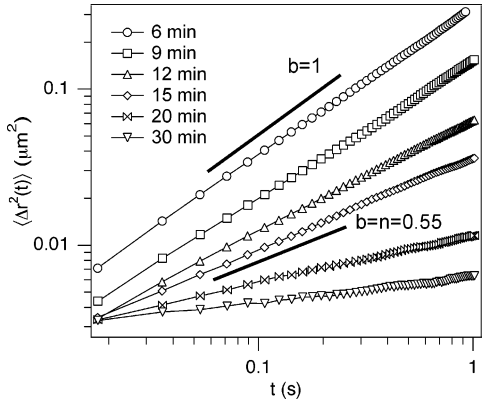

Figure 2. Ensemble-averaged mean-squared displacement vs time for 1 μm PS tracer particles embedded in 0.15% MAX1. The individual data sets represent measurements at various times after the initiation of the folding and self-assembly process ($t = 0$ min). The line with a logarithmic slope $b = 1$ is the expected response for a purely viscous behavior, while $b = n = 0.55$ indicates the dynamics at the gel point.

The molar extinction coefficient, ϵ_{220}, was determined by amino acid analysis. Prior to the start of the experiment, 125 μL of pH 9 buffer (250 mM Borate and 20 mM NaCl) was equilibrated in a 1 mm quartz cell at 22 °C in the cell holder for 5 min. Peptide stock was added to the cell to obtain a final volume of 250 μL and the required peptide concentration. The contents were gently mixed by inverting the sample several times and quickly placed in the cell holder. The experiment was started immediately and CD signal at 216 nm was recorded at 1 min intervals for 90 min. At the end of 90 min, a wavelength scan was done from 260 to 190 nm. The mean residue ellipticity $[\theta]$ was calculated from $[\theta] = (\theta_{obs}/10lcr)$, where θ_{obs} is the measured ellipticity in millidegrees, l is the length of the cell (centimeters), c is the peptide concentration (molar), and r is the number of residues.

III. Results and Discussion

A. Microrheology. 1. Mean-Squared Displacement. The mean-squared displacment of probe particles, measured using multiple particle tracking, initially exhibit diffusive behavior after inducing the folding of MAX1. As time progresses, the particle motion becomes increasingly subdiffusive, until the motion is almost completely arrested. Figure 2 shows an example of this behavior for 0.15 wt % MAX1. At this concentration, weak gels result ($G_0 \sim 1$ Pa). In contrast to the gels formed at higher concentrations (2 wt % results in gels with $G_0 \sim 1600$ Pa.) Importantly, at dilute concentrations, the kinetics are more easily monitored, since for a self-assembly process, the rate is dependent on the peptide concentration. In this experiment, gelation is initiated by adjusting the pH from 4 to 9. Measurements are taken for 10 s at specific times after the initiation of folding. The mean-squared displacement $\langle \Delta r^2(t) \rangle$ is then calculated from particle trajectories. Six minutes after folding is induced, the mean-squared displacement has a slope of 1, indicating purely viscous response of the surrounding material. At $t = 9$ min, the mean-squared displacement is still diffusive, but a decrease in the magnitude indicates a higher viscosity. Beyond 9 min, Figure 2 shows that the slope of the mean-squared displacement decreases. Now, $\langle \Delta r^2(t) \rangle$ exhibits subdiffusive power-law behavior, with a decreasing logarithmic slope or scaling exponent b. When the slope reaches zero, an elastic solid with elastic modulus G_0 has formed. The mean-squared displacement at this point is $\langle \Delta r^2 \rangle \approx k_B T/6\pi a G_0$. As shown in Figure 2, the transition from a viscous fluid to an elastic solid is continuous.

In Figure 3A, we plot the results of laser tweezer microrheology measurements made after the gel has fully formed. The

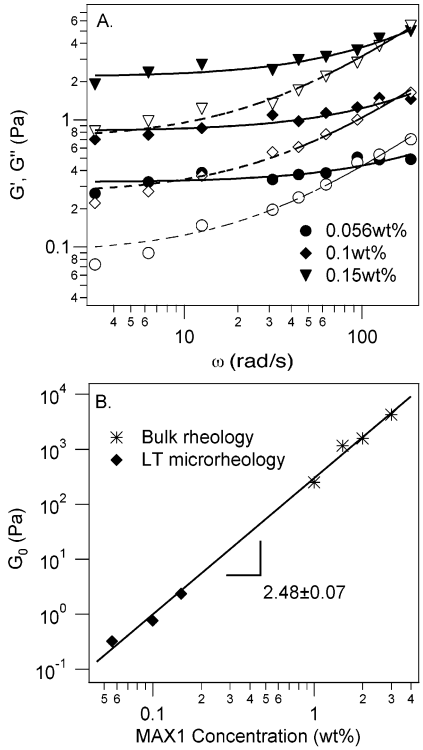

Figure 3. (A) Laser tweezer microrheology experiments of MAX1 using 1 μm probe particles after the gel has fully formed. Closed and open circles represent the storage moduli G' and loss moduli G'' calculated using eqs 4 and 5, respectively. (B) Laser tweezer microrheology (solid diamonds) and bulk rheological (stars) measurements of the MAX1 low-frequency plateau modulus. The data are fitted with a line with slope 2.48 ± 0.07.

storage modulus dominates the response, as expected, reaching a plateau at low frequencies. As shown in Figure 3B, the plateau modulus G_0 ranges between 0.3 and 2.4 Pa for peptide concentrations between 0.056 and 0.15 wt %. Also plotted in Figure 3B is the bulk rheological data obtained by Ozbas et al. for MAX1 at higher concentrations.[23] The bulk and micro experiments are in excellent agreement. The laser tweezer measurements extend the previously measured scaling dependence on concentration, $G_0 \sim c^{2.5}$. This demonstrates the important fact that the microrheological measurements using 1 μm PS microspheres are in agreement with bulk rheological experiments for the conditions used in this study and confirms that the rheology of MAX1 is consistent with that of cross-linked semiflexible filaments over 2 decades in peptide concentration.[23]

2. Determination of the Gelation Time. Before examining the kinetics of assembly at other concentrations, a clear definition of the gelation time must be established. The critical gel is the point at which the growing structure first percolates the entire sample; it has the unique property that the creep compliance exhibits a power-law scaling over all times

$$J_c(t) = \frac{\sin n\pi}{n\pi S} t^n \qquad (6)$$

where S is the gel strength with units Pa·s^n and n is the critical scaling exponent.[37,38] Power law behavior arises from the fractal-like structural self-similarity of the network that defines the critical gel. At the gel point, the probe particle mean-squared displacement, as defined by eq 1, should exhibit the same scaling exponent n with time as defined by eq 6 (e.g., $\langle \Delta r^2(t) \rangle_c \sim t^n$). The gel point in Figure 2 is therefore identified when the

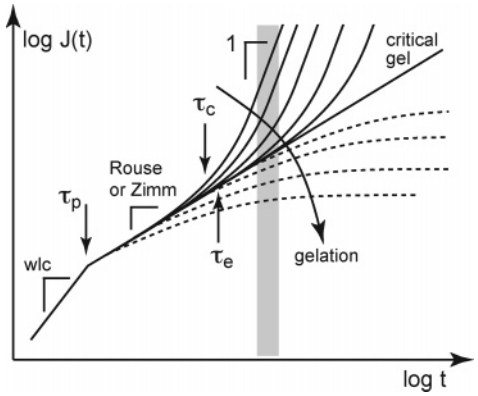

Figure 4. Anticipated creep compliance for MAX1. A crossover from wormlike chain (wlc) dynamics to Rouse or Zimm dynamics occurs on time scales longer that τ_p, the characteristic time of fluctuations on wavelengths of the MAX1 filament persistence length. The longest relaxation times of the gel before the gel point (τ_c) and after the gel point (τ_e) are indicated by the arrows. At the gel point, $J(t)$ exhibits power-law behavior over all times greater than τ_p. The gray box represents the lag time window of microrheology measurements using multiple particle tracking.

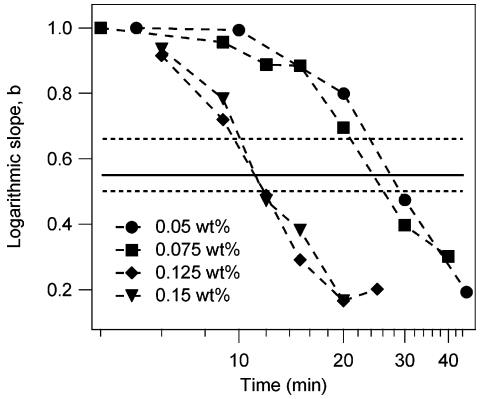

Figure 5. Logarithmic slope b of the mean-squared displacement as a function of time for 1 μm PS microspheres. The abscissa represents time points of microrheological measurements taken after the initiation of the folding and self-assembly process. The time at which each curve crosses $b = n = 0.55$ identifies the gelation time, t_g. The lower dashed line indicates $b = 0.5$, while the upper dashed line shows $b = 0.7$.

logarithmic slope b of the mean-squared displacement with time reaches n ($b = \mathrm{d}\ \ln\langle\Delta r^2(t)\rangle/\mathrm{d}\ \ln t$).

Unfortunately, an universal value for the critical gel scaling exponent n has remained elusive.[39] In fact, n is reported to range significantly, depending on the molecular architecture of the precursor molecules and the structure of the critical network. For example, bacterial polyesters formed by *Pseudomonas oleovorans* exhibit $n = 0.11$,[40] while for end-linked poly(dimethylsiloxane) polymers in the presence of a diluent, n can be as high as 0.92.[41] However, in the case of MAX1, a narrower range is expected due to the fact that the underlying polymer filament structure and dynamics should behave as either Rouse-like random coils or Zimm-like self-avoiding coils. As we discuss below, this results in a reasonable range of n between 0.5 and 0.7 at the gel point.

Figure 4 represents the creep compliance for MAX1 as it gels. It is known that MAX1 assembles into a physically cross-linked network of semiflexible filaments with an estimated persistence length $L_p \approx 50$ nm.[23] Therefore, on time scales shorter than those associated with the undulations of filaments on wavelengths of the persistence length L_p, $t \ll \tau_p \sim \xi_p L_p^3/k_BT$, where ξ_p is the filament friction per unit length, the growing hairpin structure should exhibit the dynamics of wormlike chains (wlc).[42]

Owing to the relatively short persistence length, there is a crossover $t > \tau_p$ that corresponds to dynamics on filament contour wavelengths greater than L_p, where the dynamics exhibit Rouse or Zimm-like behavior for a fractal cluster.[39] For the pregel, this scaling behavior extends to τ_c, reflecting the longest relaxation time of the largest cluster. As clusters grow, the crossover to the relaxation regime dominated by the diffusion of clusters for $t > \tau_c$ occurs at longer times, until the growing structure percolates the entire sample. At this point, the longest relaxation time diverges, giving rise to the power-law behavior described by eq 6. Beyond the gel point, a new longest relaxation time emerges, τ_e, corresponding to a plateau due to increasing numbers of filaments and cross-links forming in the percolated structure (dashed lines in Figure 4). The plateau onset time τ_e decreases as the length between cross-links decreases.[42]

Our microrheology measurements are consistent with the above behavior, considering the relatively small window of time scales that are sampled from the overall relaxation behavior using multiple particle tracking. The gray box in Figure 4 represents the time range of the experiments. We expect to see an initial drop in the magnitude of $\langle\Delta r^2(t)\rangle$, followed by a gradual change in slope as the terminal relaxation time first increases due to the increasing size of the growing clusters and then decreases once again as the number of entanglements and cross-links in the network increase. This is indeed observed for the mean-squared displacements of probe particles in MAX1, as shown in Figure 2. At a minimum, $n = 0.5$ reflects the value we expect for Rouse-like behavior of the percolated filament structure.[43] Values $n = 0.67$ and $n = 0.55$ correspond to those expected for Zimm behavior for random coils and self-avoiding coils, respectively. Given the low MAX1 concentrations and short persistence length, the value $n = 0.75$, corresponding to wormlike chain dynamics, is unlikely. That is, $L \gg L_p$ at the percolation point. From here on, we use $n = 0.55$, since it has been shown that other semiflexible polymers in the coil-like limit, notably DNA, are not free draining.[44] We are currently developing microrheology experiments that will measure the mean-squared displacement over a much wider range of time scales. This will enable the precise determination of n for these peptide systems.

The application of the GSER (eq 1) assumes that the probe particles experience a locally uniform material on a length scale comparable to their radius. Although it is expected to hold at either limit of the fluid−gel transition (cf. the agreement between bulk and microrheology demonstrated in Figure 3 for the final gel), the GSER may not be valid through the entire transition. For instance, if the mesh size at some point during gelation is larger than the average probe radius, the dynamics will reflect the diffusion in a heterogeneous network, rather than the viscoelastic response.[45] The fast gelation kinetics of MAX1 minimize the uncertainty this causes when identifying the gel point, but this may not hold for all materials. Below, we discuss this further in the context of our results obtained using different probe sizes and surface chemistries.

Figure 5 shows the logarithmic slope b of different MAX1 concentrations between 0.05 and 0.15 wt % as a function of time. As discussed above, the point at which $b = n = 0.55$ is taken as the gel point at each concentration, and defines the gel time t_g, while the dashed lines indicate the range of possible values for n. At higher peptide concentrations, the self-assembly process is faster, as expected, and the movements of the tracer particles are constrained by the hydrogel network at shorter times than for lower peptide concentrations. The lowest concentrations

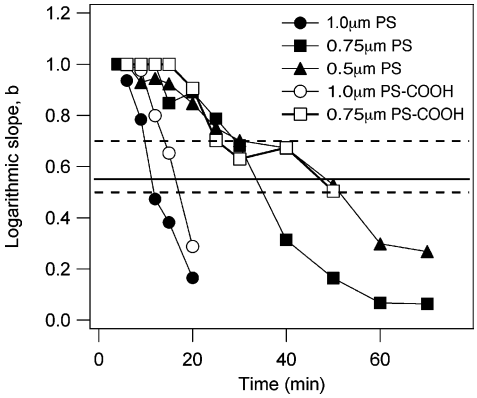

Figure 6. Logarithmic slope b of the mean-squared displacement as a function of time for 1.0 and 0.75 μm PS microspheres and 1.0 μm carboxylated PS (PS-COOH) probes. The abscissa represents time points of microrheological measurements taken after the initiation of the folding and self-assembly process. The time at which each curve crosses $b = n = 0.55$ identifies the gelation time, t_g. The lower dashed line indicates $b = 0.5$, while the upper dashed line shows $b = 0.7$.

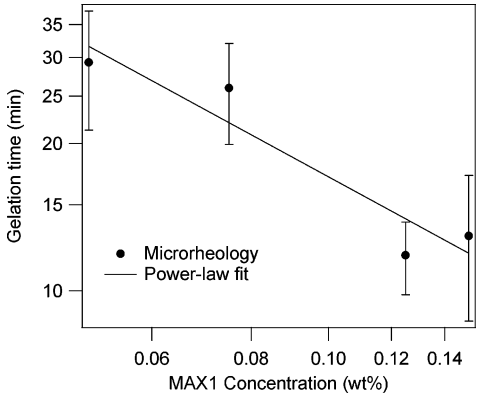

Figure 7. Gelation time t_g vs MAX1 concentration. Each point is an average of at least three experiments. The error bars reflect the standard deviation of the measurements and uncertainty with respect to the critical gel exponent n. The line is a power-law fit $t_g = kc^{\nu}$ with $\nu = -0.9 \pm 0.2$ and $k = 2.2 \pm 1.7$ min.

exhibit viscous behavior for up to 12 min after peptide folding is initiated; at this time higher concentrations have already formed a percolated network. Importantly, knowledge of how t_g varies with concentration allows one to predict the gelation times for any concentration of MAX1, facilitating applications in which the onset of gelation is critical.

To evaluate the effects of probe particle size and surface chemistry, the results of microrheology experiments in 1 wt % MAX1 conducted with 0.75 and 0.5 μm PS probes, as well as 1.0 and 0.75 μm carboxylated PS microspheres (PS-COOH), are shown in Figure 6. Comparing the PS and PS-COOH results, we find a dependence on particle surface chemistry for the smaller 0.75 μm probes, while the effect is consistent, but much weaker, for 1.0 μm microspheres. In the former case, 0.75 μm PS-COOH particles exhibit diffusive behavior for a longer time before the motion becomes subdiffusive. The resulting gel time appears to be longer for these particles when compared with 0.75 μm PS particles. For 1 μm particles, the times at which $b = 0.55$ are nearly identical between PS and PS-COOH particles. These results demonstrate that microrheological measurements of gelation kinetics are likely to depend on the detailed structure of the incipient gel, and the use of multiple particle sizes and surface chemistries provides more information on this structure. In MAX1, the structural length scales at the gel point are small enough that 1 μm diameter particles, regardless of the surface chemistry, demonstrate identical behavior. In contrast, the structure of the incipient gel still provides enough free volume for particles smaller than 1 μm to move significantly. As the hairpin filaments continue to grow, entangle, and cross-link, the small particles are eventually constrained more tightly in the network. However, even at long times (i.e., at 70 min), the mean-squared displacements at for 0.75 and 0.5 μm PS particles still exhibit the logarithmic slopes $b = 0.06$ and 0.27, respectively, compared with the purely elastic response ($b \approx 0$) of 1 μm for particles measured using laser tweezers. This indicates that the gel network is still fairly open on submicrometer length scales at these low concentrations.

In addition, we note that the role of interactions between the probe and material in microrheology experiments are an important matter and of great interest. The experiments of McGrath and Kuo,[46] Valentine et al.,[47] and our previous work[48,49] show that the microrheological response depends strongly on the surface chemistry of the probes. From these studies, it is known that "passivated" particles become increasingly insensitive to the material and produce microrheological results which differ from bulk measurements. This is due to entropically driven depletion layers that form around the probes, thus altering the response due to a locally heterogeneous polymer fluid structure.[48,49] This has also been observed for entangled solutions of DNA, where a depletion layer was found to scale with the mesh size.[50] In fact, most microrheology measurements reported in the literature have been performed with surface chemistries that interact strongly with the material. Provided that particles do not cause the percolation of the network, which is unlikely at the low particle volume fractions used, interactions are beneficial in order to probe the development of the gel structure.

The gel times t_g at each concentration are plotted in Figure 7. Each point represents multiple measurements, and the error bars reflect not only the standard deviation of t_g measurements but also the uncertainty with respect to the critical gel exponent n illustrated by the dashed lines in Figure 5. The gel time t_g decreases as the peptide concentration increases, from ~30 min for 0.05 wt % to 11 min for 0.15 wt %.

The power-law expression

$$t_g = kc^{\nu} \tag{7}$$

where c is the peptide concentration in weight percent, provides a reasonable description of the gel time, as shown in Figure 7. From a least-squares fit, we find $\nu = -0.9 \pm 0.2$ and $k = 2.2 \pm 1.7$ min. These results provide an empirical basis for controlling the assembly time of the hydrogel networks based on concentration. Furthermore, extrapolating the model yields physically reasonable values at higher peptide concentrations. For instance, Schneider et al. report that the storage modulus measured using bulk rheology far exceeds the loss modulus for 2 wt % MAX1, even at the earliest times that could be measured after triggering the self-assembly.[1] This is consistent with a calculated gel time of ~1 min at 2 wt % MAX1 using eq 7 with the fitted parameters.

B. Circular Dichroism. The kinetics of folding and self-assembly at the molecular level are characterized using CD spectroscopy. In Figure 8A, we plot the far-UV wavelength spectra for peptide concentrations between 0.003 and 0.15 wt %, recorded after 90 min. Even at this prolonged time, apparent equilibrium has not been reached for the more dilute samples (e.g., 0.05−0.1 wt %). MAX1 samples with very low concentrations ($c \leq 0.011$ wt %) remain unfolded. This indicates that folding and self-assembly is disfavored at low peptide concen-

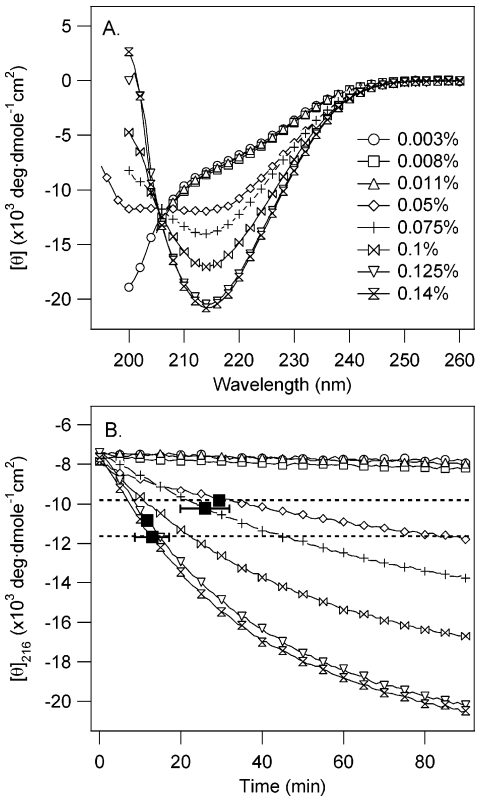

Figure 8. Results of CD measurements for various concentrations of MAX1 at pH 9, 22 °C: (A) far-UV CD spectra for various concentrations MAX1 after 90 min; (B) $[\theta]_{216}$ monitored as a function of time. The solid black squares represent t_g, measured using microrheology.

trations and reflects the coupled equilibria in the hierarchical self-assembly. This interesting feature will be discussed in greater detail elsewhere.

For MAX1 concentrations $c \geq 0.05$ wt %, the folding and self-assembly that leads to β-sheet formation increases with time. This is seen clearly by plotting mean residue ellipticity at 216 nm ($[\theta]_{216}$) as a function of time for peptide concentrations between 0.003 and 0.15 wt % in Figure 8B. The rate of β-sheet formation increases with increasing MAX1 concentration, which reflects a faster rate of the self-assembly process.

As mentioned previously, filament formation and subsequent gelation are fully dependent on the folded state of the peptide, implying a direct relationship between the extent of β-sheet formation measured by CD spectroscopy to the evolution of network structure. Because it is impossible to distinguish the separate contributions to the CD spectra from the folded monomer and assembled network, CD spectroscopy alone cannot be used to determine the time that a structurally percolated hydrogel network is reached. Since microrheology is sensitive to the formation of the filamentous microstructure, and fairly insensitive to the folding transition itself, it provides unique information on the assembly kinetics of the peptide network. When we superimpose the gel times determined from microrheology onto the CD data, shown by the solid black squares in Figure 8B, we find that the gel time corresponds to a narrow window of $[\theta]_{216}$ values between -10×10^3 and -12×10^3 deg dmol^{-1} cm^2. This represents the minimum amount of β-sheet structure that is necessary to form a percolated microstructure that defines a critical gel.

Interestingly, there are a few examples of published CD spectra of model, monomeric β-hairpins[51,52] and three-stranded antiparallel β-sheets[53] that are similar in sequence length to MAX1 and have no or few aromatic side chains that contribute to the far-UV CD. In aqueous solution, these systems exhibit spectra with minima centered at 216−218 nm, as expected.[54] However, their mean residue ellipticities at these wavelengths range from −1500 to −5000 deg dmol^{-1} cm^2, well below the magnitude of values exhibited by MAX1 (−10 000 to 12 000) that defines the self-assembled percolated network. This suggests that for de novo design efforts aimed at generating monomeric hairpins or sheet containing structures the magnitude of $[\theta]_{216-218}$ can be used to rapidly assess self-assembly leading to soluble aggregates before more timely sedimentation analytical ultracentrifugation experiments are initiated. It should be noted that CD has classically been used to investigate a peptide's propensity toward self-assembly by acquiring concentration-dependent spectra; spectra of increasingly concentrated samples reported in terms of mean residue ellipticity (therefore normalized for concentration) that do not vary in magnitude are normally interpreted as nonassociating systems. Figure 6a indicates that as the concentration is increased, $[\theta]_{216-218}$ indeed increases. However, even after 12 h (data not shown) these samples are still not at equilibrium, and further increase in $[\theta]_{216-218}$ is very slow. This results in the appearance of a concentration-dependent system. Inspection of the 0.125 and 0.15 wt % data in Figure 8 indicates that these samples are at apparent equilibrium. Here, the magnitude of $[\theta]_{216-218}$ plateaus and becomes invariant with concentration and most likely reflects the folded baseline for samples which have not yet reached equilibrium. Taken together, these data suggest that assessing a newly designed peptide's aggregation state solely on the basis of concentration-dependent CD studies may be misleading and that the overall magnitude of $[\theta]_{216-218}$ may be a good indicator of self-assembly, at least for β-systems having few aromatics that have similar sequence lengths as MAX1.

IV. Conclusions

Microrheology has proven useful for studying the hydrogelation of small peptides because it expands the lower concentration range of rheological measurements. Under these conditions, gelation is slow enough that the assembly kinetics of the fibrillar network can be monitored, including the point at which a critical gel forms. Because the rheological response is dependent solely on the developing macromolecular network and is insensitive to the peptide folding transition, it provides unique and critical information that is complementary to spectroscopic studies.

Using microrheology, we have shown that a simple power law is sufficient for modeling the kinetics of hydrogel formation. This can be used to tailor the concentration-dependent responsiveness of MAX1. Furthermore, the results provide an empirical relationship between the gel time and the mean residue ellipticity monitored at 216 nm by far-UV CD. The gel point was found to correspond to values of $[\theta]_{216}$ between -10×10^3 and -12×10^3 deg dmol^{-1} cm^2. This provides a means of monitoring gel formation purely by spectroscopy, aiding in rapidly establishing peptide sequence−material formation relationships.

Acknowledgment. The authors thank Becky Gable for her help with the experiments. This work was supported by NIH Grant 2 P20 RR016472-04 under the INBRE program of the National Center for Research Resources. E.M.F. also acknowledges support from NIH/NIBIB under Grant R01 EB003172-01. C.V. thanks the Netherlands Organization for Scientific Research (NWO) for funding via a Talent fellowship, and J.P.S. acknowledges the NSF for support (CHE-0348323). C.S. was supported by the Army Research Laboratory under the ARMAC-RTP Cooperative Agreement No. DAAD19-01-2-0001. CDV

References and Notes

(1) Schneider, J.; Pochan, D.; Ozbas, B.; Rajagopal, K.; Pakstis, L.; Kretsinger, J. *J. Am. Chem. Soc.* **2002**, *124*, 15030−15037.
(2) Zhang, S. *Nat. Biotechnol.* **2003**, *10*, 1171−1178.
(3) Collier, J. H.; Hu, B.-H.; Ruberti, J. W.; Zhang, J.; Shum, P.; Thompson, D. H.; Messersmith, P. B. *J. Am. Chem. Soc.* **2001**, *123*, 9463−9464.
(4) Nowak, A.; Breedveld, V.; Pakstis, L.; Ozbas, B.; Pine, D.; Pochan, D.; Deming, T. *Nature (London)* **2002**, *417*, 424−428.
(5) Aggeli, A.; Bell, M.; Boden, N.; Keen, J. N.; Knowles, P. F.; McLeish, T. C. B.; Pitkeathly, M.; Radford, S. E. *Nature (London)* **1997**, *386*, 259−262.
(6) Petka, W.; Harden, J.; McGrath, K.; Wirtz, D.; Tirrell, D. *Science* **1998**, *281*, 389−392.
(7) Qu, Y.; Payne, S. C.; Apkarian, R. P.; Conticello, V. P. *J. Am. Chem. Soc.* **2000**, *122*, 5014−5015.
(8) Lee, J.; Macosko, C.; Urry, D. *Macromolecules* **2001**, *34*, 4114−4123.
(9) Tang, A.; Wang, C.; Stewart, R. J.; Kopeæek, J. *J. Controlled Release* **2001**, *72*, 57−70.
(10) Hartgerink, J. D.; Beniash, E.; Stupp, S. I. *Proc. Natl. Acad. Sci. U.S.A.* **2002**, *99*, 5133−5138.
(11) Beebe, D. J.; Moore, J. S.; Bauer, J. M.; Yu, Q.; Liu, R. H.; Devadoss, C.; Jo, B. H. *Nature (London)* **2000**, *404*, 588−590.
(12) Eddington, D. T.; Beebe, D. J. *Adv. Drug Delivery Rev.* **2004**, *5*, 199−210.
(13) Peppas, N.; Bures, P.; Leobandung, W.; Ichikawa, H. *Eur. J. Pharmacol. Biopharm.* **2000**, *50*, 27−46.
(14) Hoffman, A. S. *Adv. Drug Delivery Rev.* **2002**, *43*, 3−12.
(15) Langer, R.; Peppas, N. A. *AIChE J.* **2003**, 2990−3275.
(16) Lee, K.; Mooney, D. J. *Chem. Rev.* **2001**, *101*, 1869−1879.
(17) Rajagopal, K.; Schneider, J. *Curr. Opin. Struct. Biol.* **2004**, *14*, 480−486.
(18) Lutolf, M. P.; Hubbell, J. A. *Nat. Biotechnol.* **2005.**
(19) Pochan, D.; Schneider, J.; Kretsinger, J.; Ozbas, B.; Rajagopal, K.; Haines, L. *J. Am. Chem. Soc.* **2003**, *125*, 11802−11803.
(20) Ozbas, B.; Kretsinger, J.; Rajagopal, K.; Schneider, J.; Pochan, D. *Macromolecules* **2004**, *37*, 7331−7337.
(21) Kretsinger, J.; Haines, L.; Ozbas, B.; Pochan, D.; Schneider, J. *Biomaterials* **2005**, *26*, 5177.
(22) Haines, L. A.; Rajagopal, K.; Ozbas, B.; Salick, D. A.; Pochan, D.; Schneider, J. *J. Am. Chem. Soc.* **2005**, *127*, 17025−17029.
(23) Ozbas, B.; Rajagopal, K.; Schneider, J. P.; Pochan, D. J. *Phys. Rev. Lett.* **2004**, *93*, 268106.
(24) Mason, T. G.; Weitz, D. A. *Phys. Rev. Lett.* **1995**, *74*, 1250−1253.
(25) Mason, T. G.; Ganesan, K.; van Zanten, J. H.; Wirtz, D.; Kuo, S. C. *Phys. Rev. Lett.* **1997**, *79*, 3282−3285.
(26) Gittes, F.; Schnurr, B.; Olmsted, P.; MacKintosh, F.; Schmidt, C. *Phys. Rev. Lett.* **1997**, *79*, 3286−3289.
(27) Schnurr, B.; Gittes, F.; MacKintosh, F.; Schmidt, C. *Macromolecules* **1997**, *30*, 7781−7792.
(28) Apgar, J.; Tseng, Y.; Fedorov, E.; Herwig, M. B.; Almo, S. C.; Wirtz, D. *Biophys. J.* **2000**, *79*, 1095−1106.
(29) Palmer, A.; Xu, J.; Wirtz, D. *Rheol. Acta* **1998**, *37*, 97−106.
(30) Mason, T. G. *Rheol. Acta* **2000**, *39*, 371−378.
(31) Ferry, J. *Viscoelastic Properties of Polymers*; Wiley: New York, 1980.
(32) Yamada, S.; Wirtz, D.; Kuo, S. C. *Biophys. J.* **2000**, *78*, 1736−1747.
(33) Tseng, Y.; An, K. M.; Wirtz, D. *J. Biol. Chem.* **2002**, *277*, 18143−18150.
(34) Crocker, J. C.; Grier, D. G. *J. Colloid Interface Sci.* **1996**, *179*, 298−310.
(35) Yamaguchi, N.; Chae, B. S.; Zhang, L.; Kiick, K. L.; Furst, E. M. *Biomacromolecules* **2005**, *6*, 1931−1940.
(36) Valentine, M.; Ou-Yang, H. *J. Phys.: Condens. Matter* **1996**, *8*, 9477−9482.
(37) Winter, H. H.; Chambon, F. *J. Rheol.* **1986**, *30*, 367−382.
(38) Winter, H. H.; Chambon, F. *J. Rheol.* **1987**, *31*, 683−697.
(39) Winter, H. H.; Mours, M. *Adv. Polym. Sci.* **1997**, *134*, 165−234.
(40) Richtering, H. W.; Gagnos, K. D.; Lenz, R. W.; Fuller, R. C.; Winter, H. H. *Macromolecules* **1992**, *25*, 2429−2433.
(41) Scanlan, J. C.; Winter, H. W. *Macromolecules* **1991**, *24*, 47−54.
(42) Morse, D. *Macromolecules* **1998**, *31*, 7044−7076.
(43) Hess, W.; Vilgis, T. A.; Winter, H. H. *Macromolecules* **1988**, *21*, 2536−2542.
(44) Quake, S. R.; Babcock, H.; Chu, S. *Nature (London)* **1997**, *388*, 151−154.
(45) Valentine, M.; Kaplan, P.; Thota, D.; Crocker, J.; Gisler, T.; Prud'homme, R.; Beck, M.; Weitz, D. *Phys. Rev. E* **2001**, *64*, 061506.
(46) McGrath, J. L.; Hartwig, J. H.; Kuo, S. C. *Biophys. J.* **2000**, *79*, 3258−3266.
(47) Valentine, M. T.; Perlman, Z. E.; Gardel, M. L.; Shin, J. H.; Matsudaira, P.; Mitchison, T. J.; Weitz, D. A. *Biophys. J.* **2004**, *86*, 4004−4014.
(48) Chae, B.-S.; Furst, E. M. *Langmuir* **2005**, *21*, 3084−3089.
(49) Huh, J. Y.; Furst, E. M. *Phys. Rev. E*, in press.
(50) Chen, D. T.; Weeks, E. R.; Crocker, J. C.; Islam, M. F.; Verma, R.; Gruber, J.; Levine, A. J.; Lubensky, T. C.; Yodh, A. G. *Phys. Rev. Lett.* **2003**, *90*, 108301.
(51) E.; S. H.; Gellman, S. H. *J. Am. Chem. Soc.* **1998**, *120*, 4236−4237.
(52) Setnièka, V.; Huang, R.; Thomas, C. L.; Etienne, M. A.; Kubelka, J.; Hammer, R. P.; Kideerling, T. A. *J. Am. Chem. Soc.* **2005**, *127*, 4992−4993.
(53) Schenck, H. L.; Gellman, S. H. *J. Am. Chem. Soc.* **1998**, *120*, 4869−4870.
(54) Woody, R. W. *Methods Enzymol.* **1995**, *246*, 34−71.

MA0609331